Relative influence of ENSO, IOD, and AMO over spatiotemporal variability of hydroclimatic extremes in Narmada basin, India

Author(s):
Singh, Shivam; Kumar, Nikhil; Kumar Goyal, Manish; Jha, Srinidhi

Relative influence of ENSO, IOD, and AMO over spatiotemporal variability of hydroclimatic extremes in Narmada basin, India

Shivam Singh [iD][a], Nikhil Kumar[a], Manish Kumar Goyal [iD][a],[*] and Srinidhi Jha[b]

[a] Department of Civil Engineering, Indian Institute of Technology Indore, Indore, India
[b] Department of Environmental Systems Science, Institute for Atmospheric and Climate Science, ETH Zurich, Zurich, Switzerland
*Corresponding author. E-mail: mkgoyal@iiti.ac.in

[iD] SS, 0000-0002-2367-0256; MKG, 0000-0001-9777-6128

ABSTRACT

The Narmada basin is one of the major river basins of Central India. The basin frequently experiences droughts and floods due to its geography and uneven topography. Therefore, it is important to understand the spatiotemporal variability of hydroclimatic extremes over the basin. Large-scale climate oscillations (LSCOs) have been observed significantly affecting the patterns of hydroclimatic extremes at the basin and continental scale. In this study, we have analysed the relative influence of LSCOs (EL Nino-Southern Oscillation (ENSO), Indian Ocean Dipole (IOD), and Atlantic multidecadal oscillation (AMO)) over hydroclimatic extremes of the Narmada basin. Precipitation, temperature, and streamflow extremes were analysed in stationary and nonstationary frameworks of generalized extreme value distribution. The precipitation extremes, PRCPTOT and R95p were observed significantly influenced by ENSO, IOD, and AMO individually whereas extreme Rx5day was relatively more influenced by ENSO and AMO individually and collectively. Temperature extremes, TXx was significantly more influenced by ENSO alone (26.47% of the region), while TNx was observed to be substantially more influenced by ENSO and AMO. The upper Narmada basin was found vulnerable to flooding and whereas the basin was projected to experience more frequent and intense heatwave-associated disasters in long term.

Key words: AMO, ENSO, hydroclimatic extremes, IOD, Narmada Basin, nonstationary

HIGHLIGHTS

- Precipitation and temperature extremes have been found to increasing historical trends over the Narmada Basin of Madhya Pradesh (India).
- Extreme indices have exhibited significant nonstationary behaviour due to large-scale climate oscillations (ENSO, IOD, and AMO).
- The upper part of the basin was observed as vulnerable to flooding whereas the whole basin is prone to frequent and intense heat waves in long term.

GRAPHICAL ABSTRACT
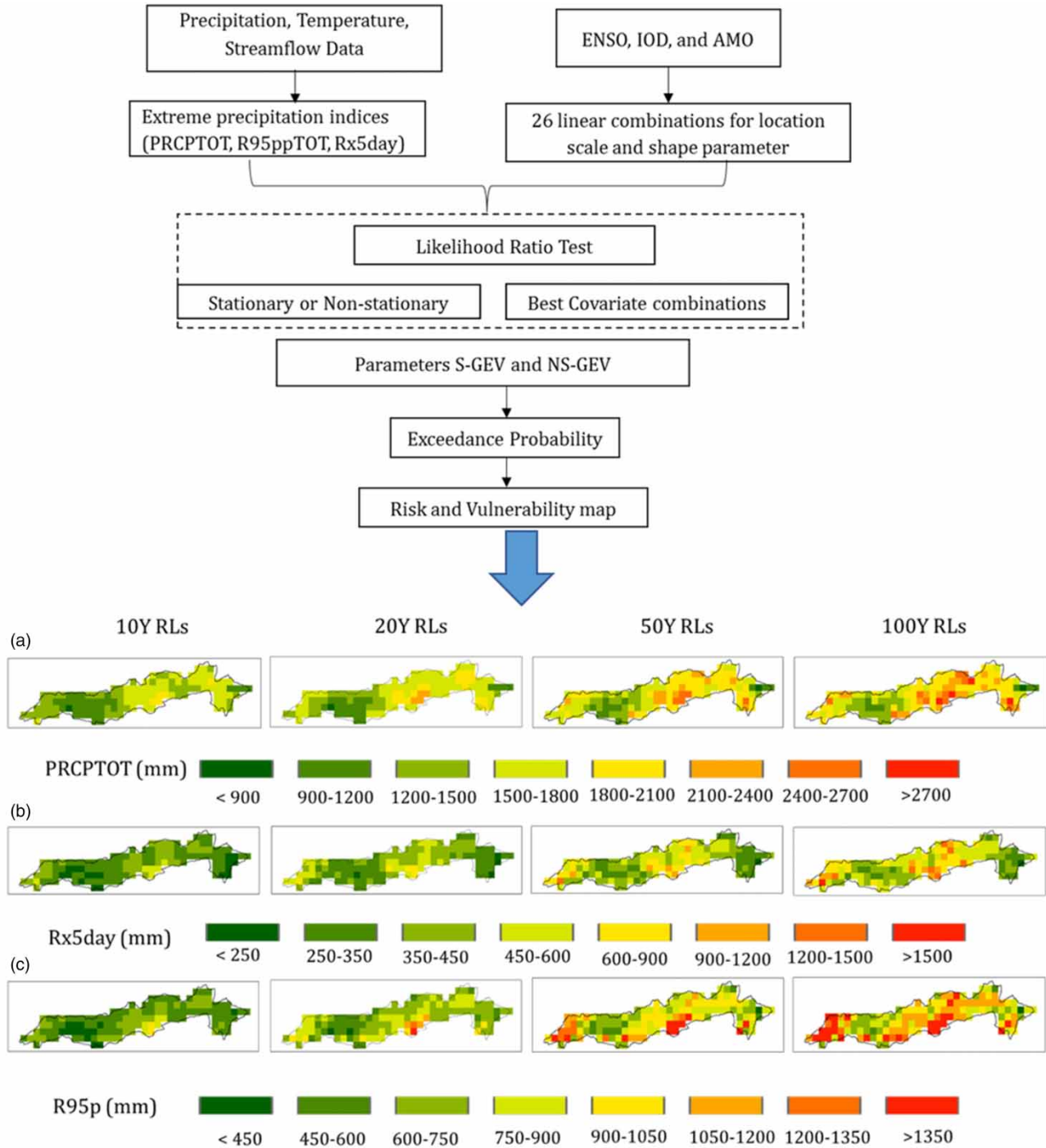
1. INTRODUCTION

Floods and droughts have been becoming more frequent in changing patterns of climate (Hirabayashi *et al.* 2008). Studies on climate model projections suggest that there will be more frequent and intense climate extremes in the projected warming future with increasing greenhouse gases emission (Canadell *et al.* 2022). Therefore, an improved understanding of the global climate system and associated extremes at the regional scale may help in reducing risk (Dai 2011; Field *et al.* 2012; Rummukainen 2012; Alfieri *et al.* 2017; Dosio *et al.* 2018; Naumann *et al.* 2018). The implications of climate change may

vary from local to global scale. Therefore, it becomes important to study the spatiotemporal variability of major hydroclimatic extremes at the basin scale for a better understanding of the impact of climate change on the local water resource system and to take consequent adaptation and mitigation measures (Panda *et al.* 2013; Garner *et al.* 2015). These hydroclimatic extremes (droughts, heatwaves, floods, etc.) significantly affect the productivity of the agriculture-dependent economy of Madhya Pradesh with rainfall as a major source of irrigation (Thomas *et al.* 2015). Apart from local factors (urbanization, orography, etc.), regional precipitation/temperature patterns have also been observed linked with large-scale climate oscillations (LSCOs) (Krishna *et al.* 1999; Saji *et al.* 1999; Rose & LaRow 2016). The LSCOs or teleconnections are recognized as a known significant connection between local hydrometeorology and large-scale oceanic-atmospheric circulation patterns, spread across the globe (Maity *et al.* 2007; Bracken *et al.* 2018; Jha *et al.* 2021). Therefore, it is important to study the relative influence of major LSCOs (EL Nino-Southern Oscillation (ENSO), Indian Ocean Dipole (IOD), and Atlantic Multidecadal Oscillation (AMO)) over hydroclimatic extremes at the basin scale to ascertain the probable variations in them.

The ENSO, coupled oceanic-atmospheric mode of the tropical Pacific Ocean, has been studied extensively across the globe for its strong influence over climate drivers (Sahu *et al.* 2012; Gao *et al.* 2017; Agilan & Umamahesh 2018; Khaki *et al.* 2018; Naveendrakumar *et al.* 2019; Song *et al.* 2019). The positive (El Nino) and negative (La-Nina) phases of ENSO cause deficit and excess rainfall over a major part of India. The extreme phases of ENSO have been found linked with extreme flooding and droughts in various regions including India across the globe (Trenberth & Guillemot 1996). Likewise, El Nino and La Nina conditions in the tropical Pacific Ocean, and the Indian Ocean also experience a physical phenomenon known as IOD. IOD is the measure of the difference in sea surface temperature (SST) between the tropical western Indian Ocean and the south-eastern Indian Ocean (Saji *et al.* 1999). The positive and negative phases of IOD represent the warming and cooling of the surface water of the Indian Ocean. The warming (cooling) phases of the tropical western Indian Ocean signify the excess (deficit) precipitation over India (Ashok *et al.* 2001; Vinayachandran *et al.* 2002). It has also been found that cool SST over the south equatorial Indian Ocean had modulated the precipitation pattern over Central India during the period 1982–2003, also the continuous warming of the tropical Indian Ocean may lead to extreme precipitation over India in the future (AjayaMohan & Rao 2008). In reference to the Indian continent, another important teleconnection is AMO which is related to North Atlantic decadal variability. The Indian summer monsoon rainfall has been found positively modulated by AMO (Ratna *et al.* 2021). For a detailed study of AMO influence over Indian summer monsoon rainfall, several other pieces of literature can be considered (Vittal *et al.* 2020; Ratna *et al.* 2021).

Climate extremes pose a fundamental threat to places, species, and people's livelihoods. Some standard methods to define extreme events are: consideration of record-breaking events (Coumou *et al.* 2013; Beniston 2015), identification of extremes from percentile-based approaches (Russo *et al.* 2015; Schär *et al.* 2016), extreme value theory (EVT). EVT has been used extensively to interpret climate extremes at regional and global scales on the basis of various standardized indices (Trenberth & Fasullo 2012; Katz 2013; Goswami *et al.* 2018; Singh *et al.* 2023). There are 27 indices available from 'climdex.org', all of which are derived from data on daily precipitation and temperature (https://www.climdex.org/learn/indices/). The expert team on climate change detection and indices (ETCCDI) of the World Climate Research Program (WCRP) has recommended these standardized indices to compare results across time periods, regions, and source datasets. Here, in this study, to analyse instantaneous and as well as cumulative responses of hydroclimatic extremes in the Narmada basin, we have taken three standard indices for precipitation (Table 1). Similar to precipitation, we have taken three indices for analysing the spatiotemporal variability of streamflow (discharge) extremes (Table 1). Central India faces extreme heat in summer that adversely affects the agricultural productivity of the region (Sharma & Mujumdar 2017; Singh *et al.* 2021). To analyse the spatiotemporal variability of extreme heat in the Narmada basin, we have also analysed three extreme indices for temperature (Table 1).

The descriptions of all nine extremes analysed in the study are mentioned in Table 1.

The spatiotemporal assessment of these indices can provide a better understanding of the risk associated with extremes (floods, droughts, heat waves, etc.) over the Narmada basin. Analysis of this link between prominent teleconnections and hydroclimatic extremes can give us a better understanding of floods, droughts, and heatwaves associated hazards (Ward *et al.* 2014; Seo *et al.* 2019). Several studies have been conducted using EVT under the stationary assumption to analyse risk due to extreme events. Under changing climate, this stationary assumption over extreme value probability distribution induces inaccuracies in the analysis of extreme events. This assumption may lead to underestimating or overestimating the probability distribution of extremes for the specific design period (Coles 2001). Therefore, a nonstationary framework would be more appropriate to assess hydroclimatic extremes accurately (Parey *et al.* 2010; Salas & Obeysekera 2014). Since ENSO, IOD, and AMO are major LSCOs that affect the patterns of hydroclimatic extremes over India, we have

Table 1 | Precipitation, temperature, and streamflow indices used in the study

	Indicator	Description/Definition
Precipitation extreme		
1.	Rx5day	Maximum consecutive 5-day precipitation
2.	R95p	Annual total rainfall from days >95th percentile
3.	PRCPTOT	Total annual precipitation
Temperature extreme		
1.	TXx	Maximum value of daily maximum temperature
2.	TNx	Maximum value of daily minimum temperature
3.	TX90p	Percentage of days when daily maximum temperature >90th percentile
Streamflow extreme		
1.	Qx1day	Daily maximum discharge
2.	Qx5day	Maximum consecutive 5-day discharge
3.	Q95p	Annual total discharge from days >95th percentile

investigated the relative influence of individual and collective response of these teleconnections at the basin scale for better assessment of risk associated with hazards. In this study, we analysed the nonstationary behaviour of extreme precipitation, temperature, and streamflow over the Narmada basin considering ENSO, IOD, and AMO as covariates in the nonstationary framework of generalized extreme value (GEV) distribution.

The specific objectives of the study are: (i) to understand the instantaneous and short-term spatiotemporal variability of hydroclimatic extremes in the Narmada basin; (ii) to identify the region of the basin more prone to different hydroclimate extremes; (iii) to understand the relative influence of ENSO, IOD, and AMO over hydro-climatology of Narmada basin.

2. DATA AND METHODOLOGY

2.1. Study area and data

Narmada river basin is the largest west-flowing river of peninsular India, with an area of 98,796 km^2 accounting for nearly 3% of the total country's area (India-WRIS 2012). The majority portion of the river basin accounts for agricultural areas, accounting for 56.90%. Most of the basin area (82%) lies in Madhya Pradesh, around 12% in Gujrat, and some part of it lies in Maharashtra (4%) and Chhattisgarh (2%) (Figure 1). As per the geography (topography) of the Narmada River basin, it has been divided into five well-defined physiographic regions: (1) The upper hilly area (Shahdol, Mandla, Durg, Balaghat, and Seoni), (2) The upper plains (Jabalpur, Narsinghpur, Sagar, Damoh, Chhidawara, Hosangabad, Betul, Raisen, and Sehore, (3) The middle plains (Khandwa, Khargone, Dewas, Indore, and Dhar), (4) The lower hilly areas (west of Nimar, Jhabua, Dhulia, Narmada and parts of Vadodara), and (5) The lower plains (Narmada, Bharuch, and parts of Vadodara). The basin mainly consists of black cotton soil. The hilly areas are well forested whereas upper, middle, and lower plains are broad and fertile. The basin experiences hydrometeorological and climatic extremes. The upper part of the catchment gets 1,000–1,850 mm of annual precipitation whereas the lower part gets only 650–750 mm.

Streamflow extreme indices were calculated using daily observed discharge data from 10 discharge stations (Mohggaon, Manot, Patan, Gadarwara, Sandia, Hoshangabad, Chhidgaon, Handia, Mandleshwar, Garudeswar) for the period of 37 years from 1979 to 2015 (Table 2). Rest stations at Narmada basin sites were discarded because of the unavailability of data for the concerned period. The discharge data have been obtained from Central Water Commission (India, WRIS). The daily rainfall data have been obtained from Indian Meteorological Department (IMD) at 0.25° resolution. The daily temperature dataset for the basin has been obtained from the Global Meteorological forcing dataset (GMFD) at 0.25° resolution.

SST anomalies over the Nino 3.4 region (17° E-120° W, 5° S-5° N) of the Central Pacific are considered as one of the potential indicators for ENSO. The monthly SST-Nino 3.4 index data were obtained from National Oceanic and Atmospheric Administration (NOAA) Centre for Weather and Climate Prediction (https://www.cpc.ncep.noaa.gov/data/indices/). IOD also referred to as Indian Nino, is an irregular oscillation of SST of the western and the eastern Indian Ocean. IOD, represented as Dipole mode Index (DMI), is the difference of SST anomalies between the tropical western Indian Ocean and
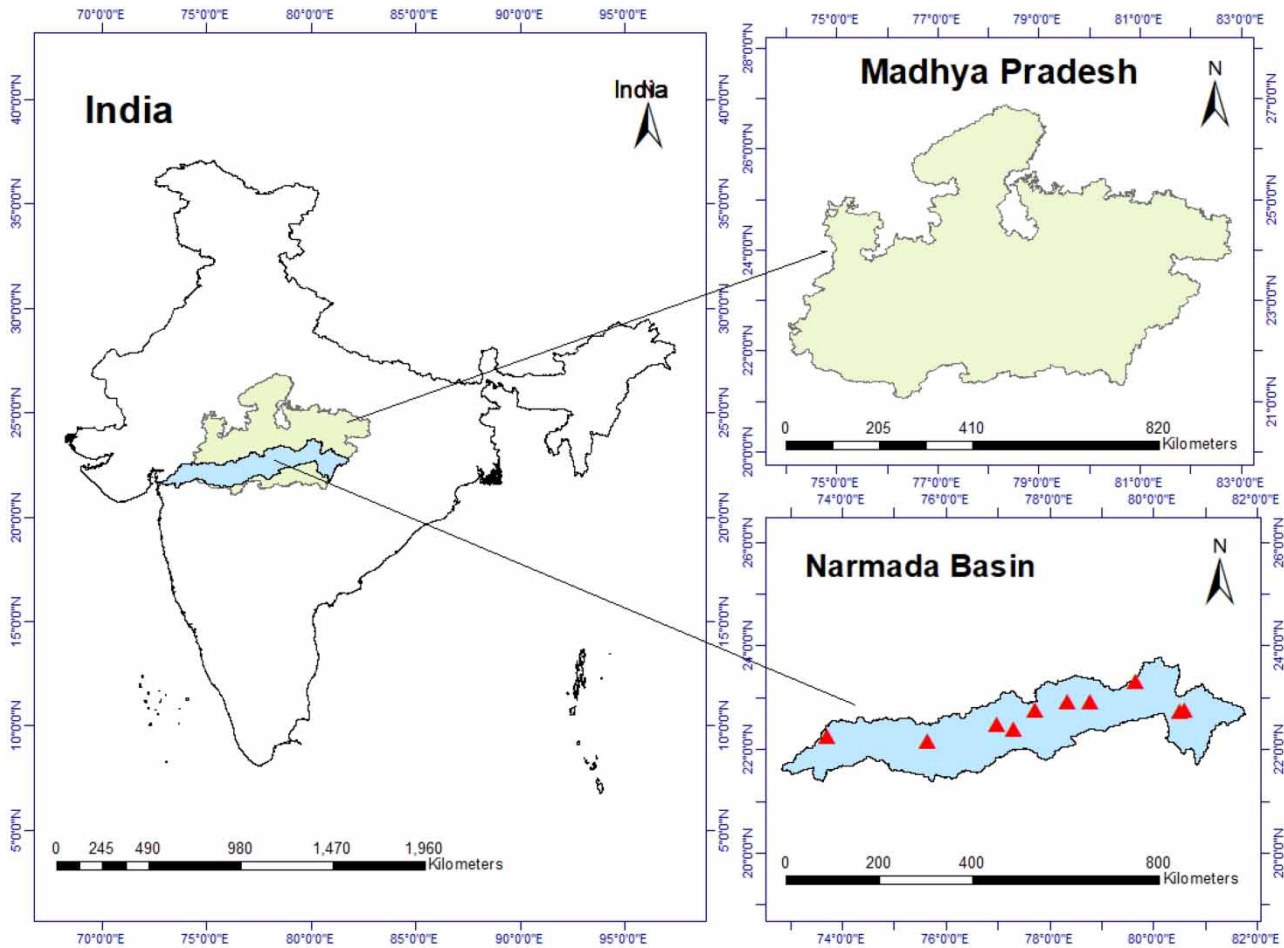
Figure 1 | Geographical location of the Narmada Basin (located majorly in Madhya Pradesh state of India and discharge stations (in red colour). Please refer to the online version of this paper to see this figure in colour: https:///dx.doi.org/10.2166/aqua.2023.219.

tropical south-eastern Indian Ocean. The monthly DMI data were obtained from Physical Science Laboratory, NOAA (https://psl.noaa.gov/gcos_wgsp/Timeseries/DMI/). Similarly, AMO data were taken from NOAA Physical Science Laboratory (https://psl.noaa.gov/data/timeseries/AMO/). These indices data have been obtained for the same period of 37 years from 1979 to 2015. As the Narmada basin receives the majority of its rainfall in the summer monsoon season,

Table 2 | Description of considered discharge stations of Narmada Basin

| S. No.	Station	Station name	Lat	Lon
1	S1	Mohggoan	22.7658	80.6228
2	S2	Manot	22.7356	80.5122
3	S3	Patan	23.3117	79.6628
4	S4	Gadarwara	22.9239	78.7917
5	S5	Sandia	22.9158	78.3475
6	S6	Hoshangabad	22.7561	77.7342
7	S7	Chhidgaon	22.4058	77.3078
8	S8	Handia	22.4903	76.9936
9	S9	Mandleshwar	22.1717	75.6608
10	S10	Garudeswar	22.265	73.7272

June–July–August–September (JJAS). Therefore, the mean values for JJAS season of LSCOs (ENSO, IOD, and AMO) were taken to analyse various extremes in the monsoon season.

2.2. Methodology

Precipitation extremes (Rx5day, PRCPTOT, R95p) and temperature extremes (TXx, TNx, TX90p), were calculated using '*climdex.pcic*' package in R studio (https://cran.r-project.org/web/packages/climdex.pcic/index.html). Similar to precipitation indices, streamflow indices (Qx1day, Qx5day, and Q95p) were also estimated using daily streamflow data collected from all 10 stations of the Narmada basin. The trend, variability, and mean distribution of precipitation, temperature extreme, and streamflow extreme indices were discussed in the Results and discussion section. These extreme indices were further investigated with the various combinations of LSCOs (ENSO, IOD, and AMO) in a nonstationary framework of EVT (Figure 2). The relative influence of these LSCOs over hydroclimatic extremes in the Narmada basin was analysed and compared from a stationary scenario.

2.2.1. Trend analysis

As discussed above, changing climate invalidates stationary assumptions and thus, affects the traditional methods of frequency analysis as well as the definitions of the return period, risks, and reliability (Pechlivanidis *et al.* 2017). Trend analysis has been carried out to understand the spatiotemporal variability of hydroclimatic extremes in the Narmada basin (Ouarda & Charron 2019). A nonparametric modified Mann Kendall (MK) trend test has been carried out using '*modifiedmk*' package of R studio to analyse monotonic trends in the data. The null hypothesis (H0) of the test is that there is no trend in the data and the alternative hypothesis (H1) is that the data follow a monotonic trend. The outputs from MK test are MK Z-statistic, Sen's slope, MK S statistics, Variance of S statistics, MK p-value, and MK's tau. The MK Z-statistics represent the level of confidence in the results of the test and Sen's slope represents the average rate of trend in the data, which have been discussed more elaborately. The statistics of the test were analysed at 5% level of significance.
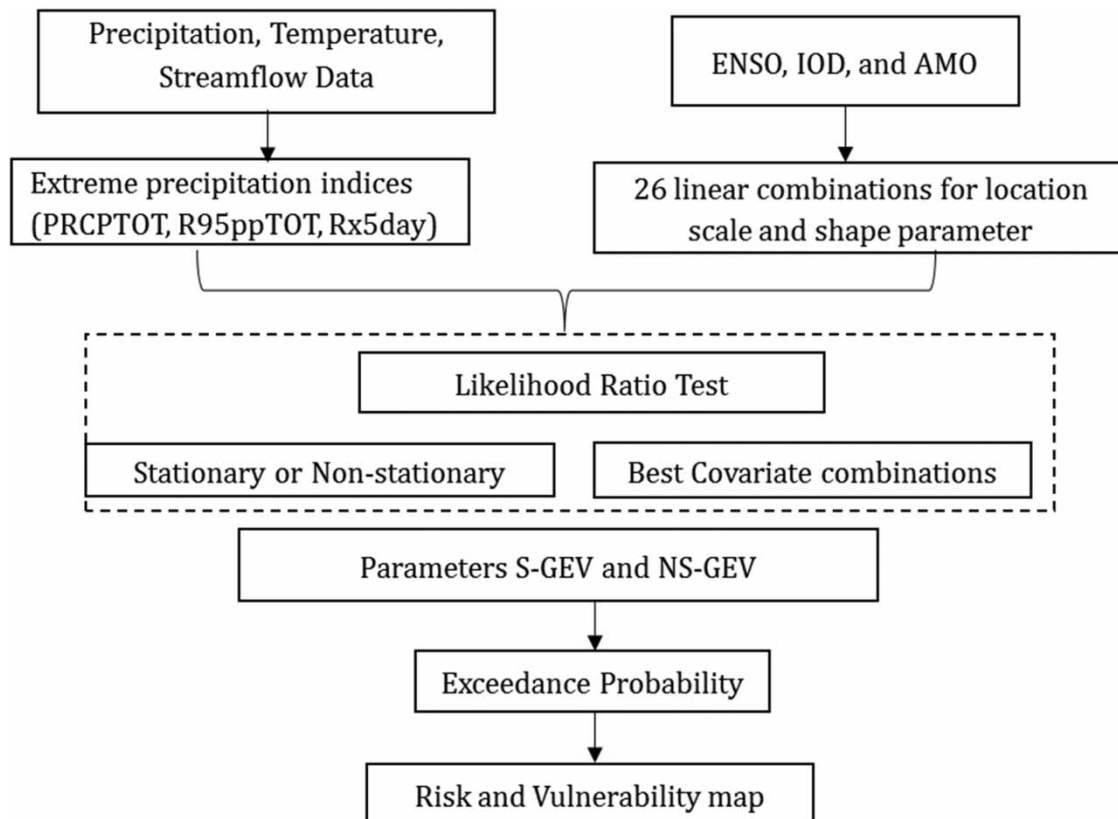
Figure 2 | Flowchart for nonstationary analysis of extreme indices with large-scale climate oscillations.

2.2.2. Nonstationary modelling

GEV distribution is popularly adopted for analysing hydroclimatic extremes. These extremes were modelled as continuous random variables in GEV distribution. The cumulative probability distribution function of the GEV distribution is given by the following equation (Katz 2013; Jha *et al.* 2021).

$$
F(x, \mu, \sigma, \xi) = \begin{cases} \exp\left\{ -\left[1 + \frac{\xi(x - \mu)}{\sigma}\right]^{\frac{-1}{\xi}} \right\}, \ \sigma > 0, \ 1 + \frac{\xi(x - \mu)}{\sigma} > 0, \ \xi \neq 0 \\ \qquad\qquad \{ \ n \text{ odd} \\ \exp\left\{ -\exp\left[-\frac{(x - \mu)}{\sigma}\right]\right\}, \ \sigma > 0, \ \xi = 0 \end{cases} \tag{1}
$$

here x is the time series of extreme indices, and μ, σ, and ξ represents the location, scale, and shape parameters of the GEV distribution, respectively. Thus, $F(x; \mu, \sigma, \xi)$ represents the cumulative distribution function (CDF) of the extreme x with parameters μ, σ, and ξ.

A total of 26 linear combinations (models) of location and scale parameters of GEV distribution were prepared using covariates ENSO, IOD, and AMO termed as C1, C2, and C3, respectively. Models formulated through various combinations of these covariates (M0, M1, M2, …) can be found in Table 3. Where M0 is the stationary model with constant parameters of GEV distribution; hence, independent of the LSCOs. However, total 26 nonstationary models (Table 3), starting from M1 to M26, in which scale and location parameters of GEV distribution have been represented as a function of covariates, are incorporated in this study. The shape parameter of the GEV distribution has been kept constant to avoid complexity in modelling (Coles 2001; Katz 2013; Yilmaz & Perera 2014; Das *et al.* 2020). The maximum-likelihood estimation (MLE) approach was used for parameter estimation from GEV distribution. Through MLE approach, the value of $\theta = [\mu, \sigma, \xi]$ has been obtained at which maximum likelihood functions attain their maximum value. Let $X = x_1, x_2, x_3, …., x(n - 1), x(n)$ be the series of any selected extreme with n number of observations. Then, the log-likelihood can be defined as (Katz 2013; Bracken *et al.* 2018):

$$
L(\theta) = -n\log - \left(1 + \frac{1}{\xi}\right) \sum_{i=1}^{n} \log\left[1 + \frac{\xi(x_i - \mu)}{\sigma}\right] - \sum_{i=1}^{n} \log\left[1 + \frac{\xi(x_i - \mu)}{\sigma}\right]^{-\left(\frac{1}{\xi}\right)}, \quad 1 + \frac{\xi(x_i - \mu)}{\sigma} > 0 \tag{2}
$$

Here, $L(\theta)$ is the likelihood function of a particular parameter vector θ. The likelihood function is the measure of how likely the dataset represents as a function of unknown parameters of distribution (GEV, in the present case) and MLE gives the values of parameters that maximize the likelihood function (Katz 2013).

The likelihood ratio test (LR test) has been used to compare the significance of the stationary and nonstationary models (Coles 2001). The hypothesis testing is carried out by comparing the minimized negative log-likelihood (nllh) of the stationary model with the nonstationary model at any particular significance level, α (0.05). Twice the difference between nllh-stationary GEV and nllh-nonstationary GEV is supposed to have an approximate Chi-squared distribution (Katz 2013). The statistics can be mathematically represented as (Jha *et al.* 2021).

$$
2[\text{nllh}_S - \text{nllh}_{NS}] > c_\alpha \tag{3}
$$

where c_α is the $(1 - \alpha)$ quantile of the Chi-square distribution. The best fit nonstationary model has been obtained based on the minimum p-value. The parameters related to the best fit model are estimated through MLE and further investigation has been carried out for the best fit model. The methodology has been presented through flowchart in Figure 2.

3. RESULTS AND DISCUSSION

3.1. Variability and trend of extreme climatic variables

Results from modified MK tests (z-statistics and Sen's slope) along with mean and standard deviation (SD) of precipitation, streamflow, and temperature extremes were analysed for the trend analysis. The Z-statistics of MK test indicate the significance in the monotonic trend of the time series of data whereas Sen's slope gives the rate of change of that time series of

Table 3 | List of total 27 models (1 stationary (M0) and 26 nonstationary) analysed in the study

Model ID	Description	Combinations of LSCOs (For location (μ) & scale (σ) parameters of GEV distribution)
M0	$X\text{-}\ GEV[\,\mu,\ \sigma,\ \xi]$	NA
M1	$X\text{-}\ GEV[\,\mu_0 + \mu1c1,\ \sigma,\ \xi]$	ENSO
M2	$X\text{-}\ GEV[\,\mu_0 + \mu2c2,\ \sigma,\ \xi]$	IOD
M3	$X\text{-}\ GEV[\,\mu_0 + \mu3c3,\ \sigma,\ \xi]$	AMO
M4	$X\text{-}\ GEV[\,\mu_0 + \mu1c1 + \mu2c2,\ \sigma,\ \xi]$	ENSO, IOD
M5	$X\text{-}\ GEV[\,\mu_0 + \mu2c2 + \mu3c3,\ \sigma,\ \xi]$	IOD, AMO
M6	$X\text{-}\ GEV[\,\mu_0 + \mu3c3 + \mu1c1,\ \sigma,\ \xi]$	AMO, ENSO
M7	$X\text{-}\ GEV[\,\mu_0 + \mu1c1 + \mu2c2 + \mu3c3,\ \sigma,\ \xi]$	ENSO, IOD, AMO
M8	$X\text{-}\ GEV[(\mu_0 + \mu1c1),\ (\sigma_0 + \sigma1C1),\ \xi]$	ENSO & ENSO
M9	$X\text{-}\ GEV[(\mu_0 + \mu1c1),\ (\sigma_0 + \sigma2C2),\ \xi]$	ENSO & IOD
M10	$X\text{-}\ GEV[(\mu_0 + \mu1c1),\ (\sigma_0 + \sigma3C3),\ \xi]$	ENSO & AMO
M11	$X\text{-}\ GEV[(\mu_0 + \mu2c2),\ (\sigma_0 + \sigma1C1),\ \xi]$	IOD & ENSO
M12	$X\text{-}\ GEV[(\mu_0 + \mu2c2),\ (\sigma_0 + \sigma2C2),\ \xi]$	IOD & IOD
M13	$X\text{-}\ GEV[(\mu_0 + \mu2c2),\ (\sigma_0 + \sigma3C3),\ \xi]$	IOD & AMO
M14	$X\text{-}\ GEV[(\mu_0 + \mu3c3),\ (\sigma_0 + \sigma1C1),\ \xi]$	AMO & ENSO
M15	$X\text{-}\ GEV[(\mu_0 + \mu3c3),\ (\sigma_0 + \sigma2C2),\ \xi]$	AMO & IOD
M16	$X\text{-}\ GEV[(\mu_0 + \mu3c3),\ (\sigma_0 + \sigma3C3),\ \xi]$	AMO & AMO
M17	$X\text{-}\ GEV[(\mu_0 + \mu1c1 + \mu2c2),\ (\sigma_0 + \sigma1C1 + \sigma2C2),\ \xi]$	ENSO, IOD & ENSO, IOD
M18	$X\text{-}\ GEV[(\mu_0 + \mu1c1 + \mu2c2),\ (\sigma_0 + \sigma2C2 + \sigma3C3),\ \xi]$	ENSO, IOD & IOD, AMO
M19	$X\text{-}\ GEV[(\mu_0 + \mu1c1 + \mu2c2),\ (\sigma_0 + \sigma3C3 + \sigma1C1),\ \xi]$	ENSO, IOD & AMO, ENSO
M20	$X\text{-}\ GEV[(\mu_0 + \mu2c2 + \mu3c3),\ (\sigma_0 + \sigma2C2 + \sigma1C1),\ \xi]$	IOD, AMO & IOD, ENSO
M21	$X\text{-}\ GEV[(\mu_0 + \mu2c2 + \mu3c3),\ (\sigma_0 + \sigma2C2 + \sigma3C3),\ \xi]$	IOD, AMO & IOD, AMO
M22	$X\text{-}\ GEV[(\mu_0 + \mu2c2 + \mu3c3),\ (\sigma_0 + \sigma3C3 + \sigma1C1),\ \xi]$	IOD, AMO & AMO, ENSO
M23	$X\text{-}\ GEV[(\mu_0 + \mu3c3 + \mu1c1),\ (\sigma_0 + \sigma1C1 + \sigma2C2),\ \xi]$	AMO, ENSO & ENSO, IOD
M24	$X\text{-}\ GEV[(\mu_0 + \mu3c3 + \mu3c1),\ (\sigma_0 + \sigma2C2 + \sigma3C3),\ \xi]$	AMO, ENSO & IOD, AMO
M25	$X\text{-}\ GEV[(\mu_0 + \mu3c3 + \mu1c1),\ (\sigma_0 + \sigma3C3 + \sigma1C1),\ \xi]$	AMO, ENSO & AMO, ENSO
M26	$X\text{-}\ GEV[(\mu_0 + \mu1c1 + \mu2c2 + \mu3c3),\ (\sigma0 + \sigma1C1 + \sigma2C2 + \sigma3C3),\ \xi]$	ENSO, IOD, AMO & ENSO, IOD, AMO

data. We have interpreted the results of Z-statistics in four categories at 5% level of significance. It was considered significantly decreasing at $Z < -1.96$, decreasing at $-1.96 < Z < 0$, increasing at $0 < Z < 1.96$ and significantly increasing at $Z > 1.96$. The rest of the three parameters (mean, SD, and Sen's slope) have been analysed into three categories based on the observation.

The spatial distribution of precipitation extreme, PRCPTOT shows that the upper part of the basin gets more precipitation and SD is also found higher in total annual precipitation at the upper half of the basin. The trend is found almost increasing over the whole basin, most importantly the lower part of the basin (Z-statistics) with an increasing (but not significantly) rate of more than 4 mm per year in the lower part of the basin. As of PRCPTOT, Rx5day and R95p were also found slightly increasing but non-significantly throughout the basin (Figure 3(a)).

A total of 10 stations (Mohggoan, Manot, Patan, Gadarwara, Sandia, Hoshangabad, Chhidgaon, Handia, Mandleshwar, Garudeswar) were taken into consideration for the streamflow and were represented as S1, S2, S3, S4, S5, S6, S7, S8, S9, and S10, respectively (Table 1). The stations have spread along the Narmada basin starting from the upper part to the tail of the river basin (Figure 1). Streamflow extremes, Qx1day, Qx5day, and Q95p for any of the stations were not found with any significant trend. Due to the contribution from various tributaries in the downstream, the streamflow of downstream stations was comparatively higher (Table 4). Q90p is the cumulative streamflow in a year from days when streamflow was more than the 90th

percentile (cumulative contribution from very high streamflow) of daily streamflow data at a station, therefore as per the definition, the magnitude of Rx5day will always be more than Rx1day and Q90p will be comparatively too high than Rx1day and Rx5day and hence the mean and Sen's slope was comparatively higher in case of Q90p (Table 4). The streamflow magnitude and consequent extremes (Qx1day, Qx5day, and Q95p) from the station (S7) installed in the tributary of the main river have also been noted with a lesser magnitude of mean and MK test statistics.

The temperature indices (TXx, TNx, and TX90p) were analysed in a similar way. There was also not any significant trend in the past in temperature extreme, TXx and TNx in the basin, i.e., the daily maximum temperature in the day and night were not significantly increasing or decreasing in the past. Another temperature extreme, TX90p, a potential indicator of heatwaves, has shown increasing throughout the basin whereas significantly increasing trend at the uppermost and lowermost parts of the basin (Figure 3(b)).

3.2. Nonstationary extreme value analysis

The distribution of extremes at all the grids/stations were checked for the nonstationarity caused by ENSO, IOD, and AMO in the extremes. LR test revealed that there was a significant amount of nonstationarity caused by LSCOs present in the extremes. Statistics of the LR test with minimum *p*-value were used to find the best combination of LSCOs influencing most of the distribution of the extremes. Rx5day shows significantly more nonstationary behaviour in majority of the basin due to LSCOs in comparison with PRCPTOT and R95p (see Supplementary Material, Figure S1) The results from the best combination of LSCO(s) (nonstationary model(s)) and stationary model were discussed in terms of return levels (RLs) of extremes at 10, 20, 50, and 100 years.
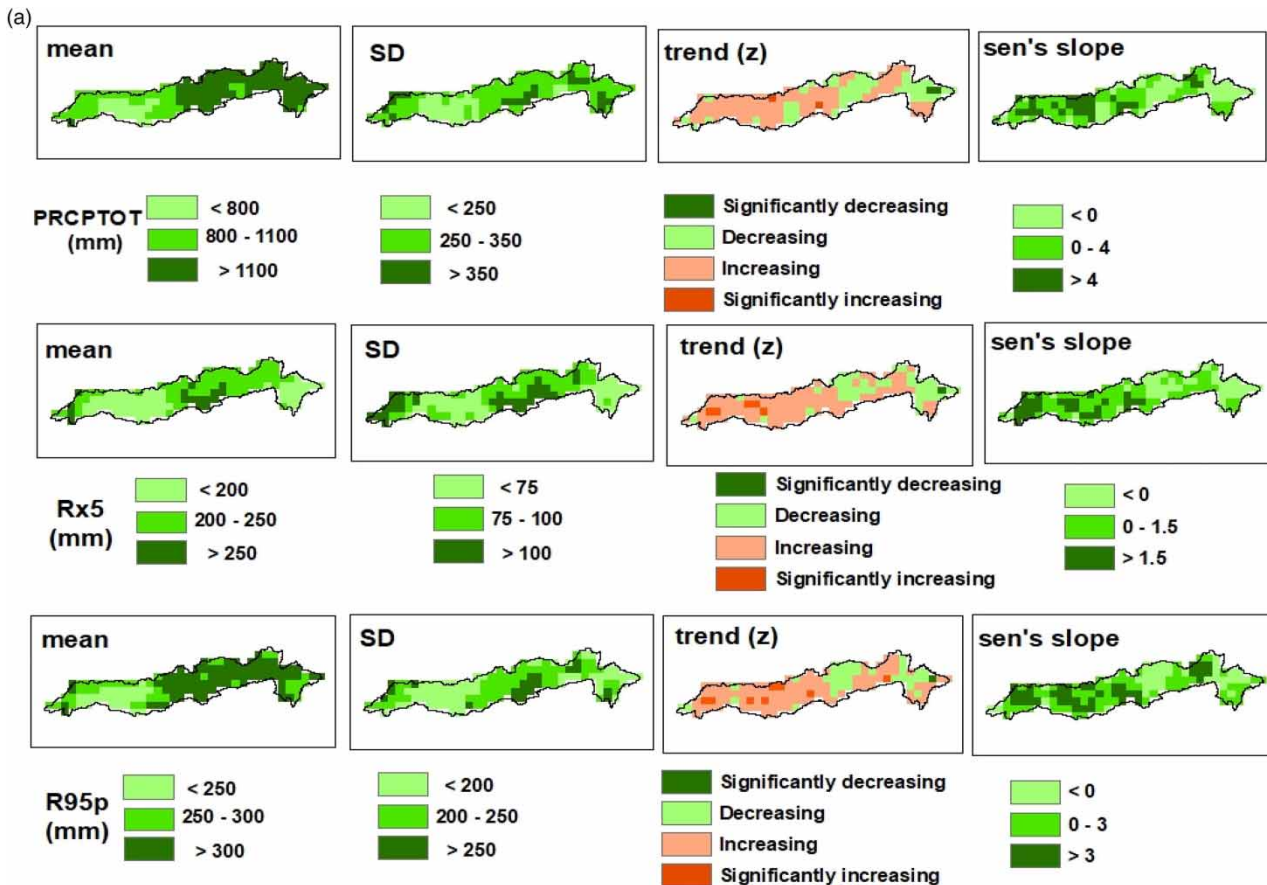
Figure 3 | (a) Mean, standard deviation, and statistics of modified MK trend test (*Z*-statistics and Sen's slope) for precipitation indices: PRCPTOT, Rx5day, and R95p (b) Mean, standard deviation, and statistics of modified MK trend test (*Z*-statistics and Sen's slope) for temperature indices (TXx, TNx, and TX90p). (*continued.*).
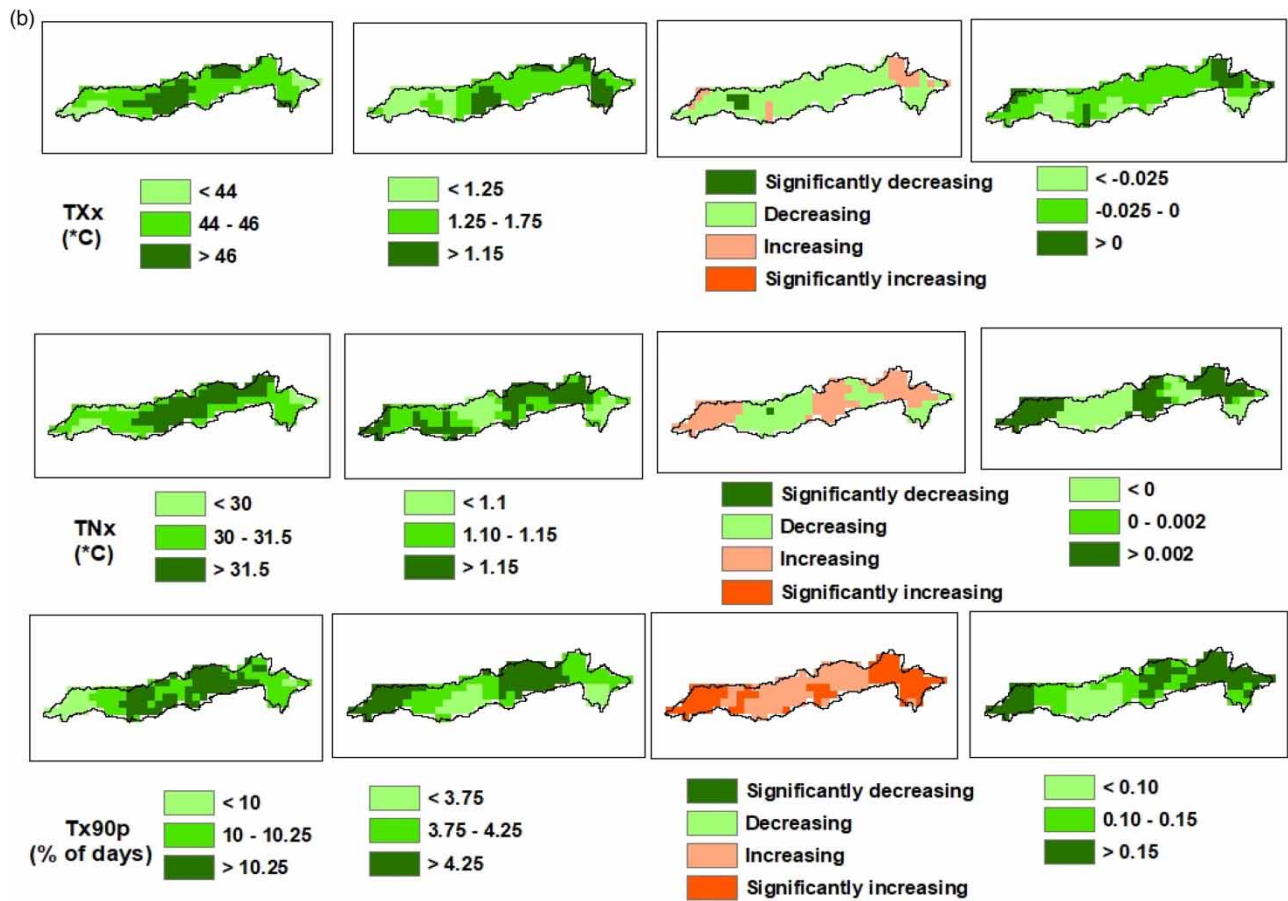
Figure 3 | Continued.

Since precipitation extreme R95p and PRCPTOT signify the cumulative response of precipitation amount, the spatiotemporal variability in these extremes was found relatively more influenced by ENSO (M1), IOD (M2), and AMO (M3) individually and have almost similar kinds of distribution in rest of the basin collectively by ENSO, IOD, and AMO (Figure 4(b) and 4(c)). In case of Rx5day, ENSO and AMO individually (M1 & M3) and collectively (M25 & M26) influence relatively more the spatiotemporal variability of the extremes in the basin (Figure 4(a)). In case of temperature extreme, the TXx in most of the Narmada basin (26.47% of the region) were found relatively more influenced by ENSO individually (Figure 4(d)) whereas TNx was found relatively more influenced by ENSO (M1) and AMO (M2) (Figure 4(e)). The temperature extreme TX90p, a potential indicator of the heatwave, was relatively more influenced by collectively ENSO with IOD and AMO (M18 & M25) (Figure 4(f)).

Since the upper half of the Narmada basin receives more precipitation, the RLs for all the extremes, PRCPTOT, Rx5day, and R95p were higher in the upper half of the basin and were found to increase (RLs) with increasing return periods (Figure 5(i)). The middle plains of the Narmada basin were experiencing a higher magnitude of precipitation extremes at high return periods and could make the region prone to flooding in the future (Figure 5(i)).

The streamflow extreme indices (Qx1day, Qx5day, and Q95p) for the basin have also been increasing with increasing return periods. The downstream stations are more sensitive because they have been influenced by the upstream tributaries (Figure 5(ii)). Also, the variance in the instantaneous streamflow extremes (Qx1day and Qx5day) of the basin was observed high in comparison with Q95p (Figure 5(ii)). The variance in Qx1day extreme of discharge for station S7, located at one of the tributaries of the main river was observed maximum (Figure 5(ii)(a)). For given streamflow extremes in almost all stations, we have found nonstationarity due to LSCOs (see Supplementary Material, Table S1).

Table 4 | Mean, standard deviation, and statistics of modified MK trend test (Z-statistics and Sen's slope) for streamflow indices (Qx1, Qx5, Q95p)

Stn No.	Indices Station name	Qx1day				Qx5day				Q95p			
		Mean	SD	Trend (Z)	Sen's Slope	Mean	SD	Trend (Z)	Sen's Slope	Mean	SD	Trend (Z)	Sen's Slope
1	Mohggoan	3,141.1	2,464.7	−1.01	−23.03	5,474.63	3,029.15	−0.60	−20.05	12,697.35	7,502.65	−0.28	−39.46
2	Manot	3,239.9	1,715.2	−1.3	−39.8	6,388.5	3,107.74	−1.38	−71.03	16,259.28	10,373.93	−2.22	−364.81
3	Patan	1,104.6	542.7	−0.99	−12.02	3,748.1	2,288.25	−0.34	−17.29	10,703.03	8,468.27	−0.83	−99.87
4	Gadarwara	1,972.3	1,188.71	−1.56	−30	3,947.02	3,016.87	−1.12	−38.46	10,126.06	7,813.64	−0.26	−22.2282
5	Sandia	9,741.7	5,766.1	−1.17	−102.9	31,06.94	20,882.9	−1.098	−345.6	75,537.08	73,474.2	−1.25	−801.43
6	Hoshangabad	13,811.3	6,673.2	−2.08	−234.3	43,347.78	28,296.03	−1.80	−693.83	110,925.1	102,214	−1.93	−2,232.26
7	Chhidgaon	2,488.5	2,117.9	−0.75	−13.46	3,842.135	2,742.72	−0.52	−15.145	7,077.02	5,668.85	0.10	3.45
8	Handia	15,419.06	6,852.1	−1.76	−224.9	48,249.92	27,497.2	−1.98	−663.6	124,598	111,568.8	−1.93	−2,062.91
9	Mandleshwar	20,838.7	11,984.5	−2.23	−349.2	59,776.26	34,705.7	−2.69	−1,252.2	151,346.1	135,844.9	−1.67	−2,758.57
10	Garudeswar	19,339.02	13,267.9	−2.47	−373.12	56,368.48	34,580.61	−3.06	−1,323.5	142,154.7	133,471.8	−2.14	−3,194.88
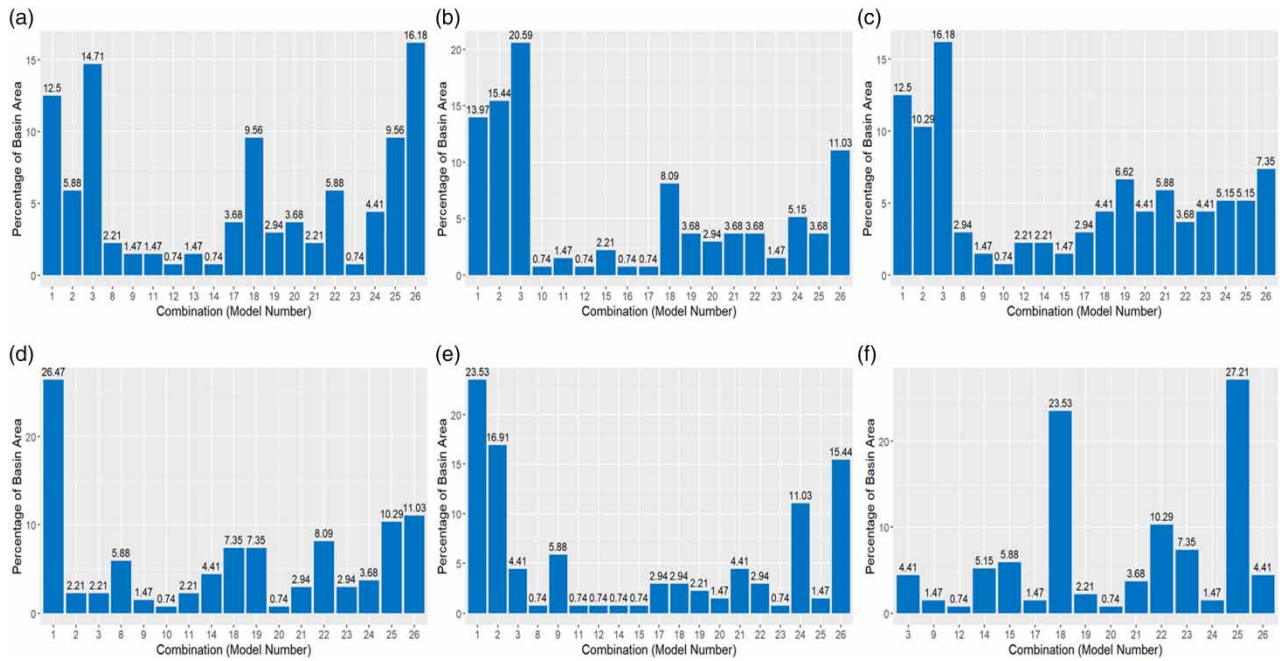
Figure 4 | Spatial extent (% of grids showing agreement in temporal variability and GEV distribution of extremes with combinations of LSCOs) of various combinations of LSCOs influencing hydroclimatic extreme (a) Rx5day, (b) PRCPTOT, (c) R95p, (d) TXx, (e) TNx, (f) TX90p.
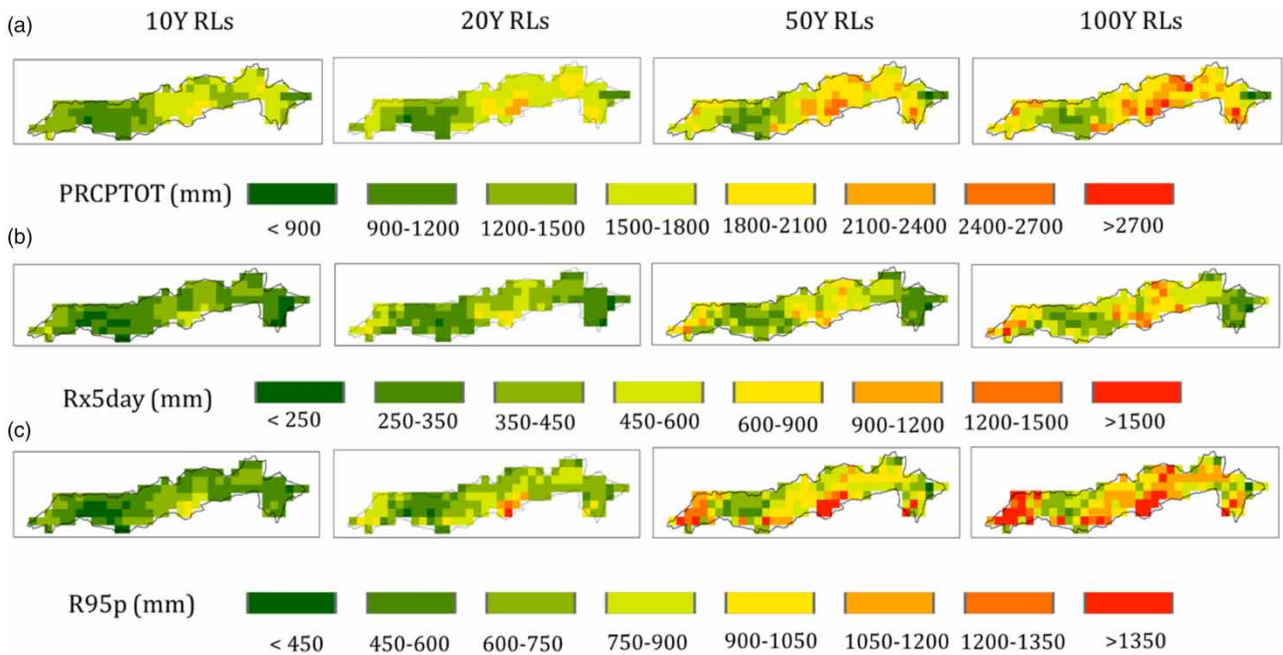
Figure 5 | (i) RLs from one of the best fit combinations of LSCOs in GEV distribution of extreme: (a) PRCPTOT; (b) Rx5day; (c) R95p at 10, 20, 50, and 100 years of return period. (ii) RLs from one of the best fit combinations of LSCOs in GEV distribution of extreme: (a) Qx1day; (b) Qx5day; (c) Q95p at 10, 20, 50, and 100 years return periods. [10y RLs refers to return level (magnitude) of extreme at 10-year return period] (iii) RLs from one of the best fit combinations of LSCOs in GEV distribution of extremes: (a) TXx; (b) TNx; (c) TX90p at 10, 20, 50, and 100 years return periods. (*continued.*).
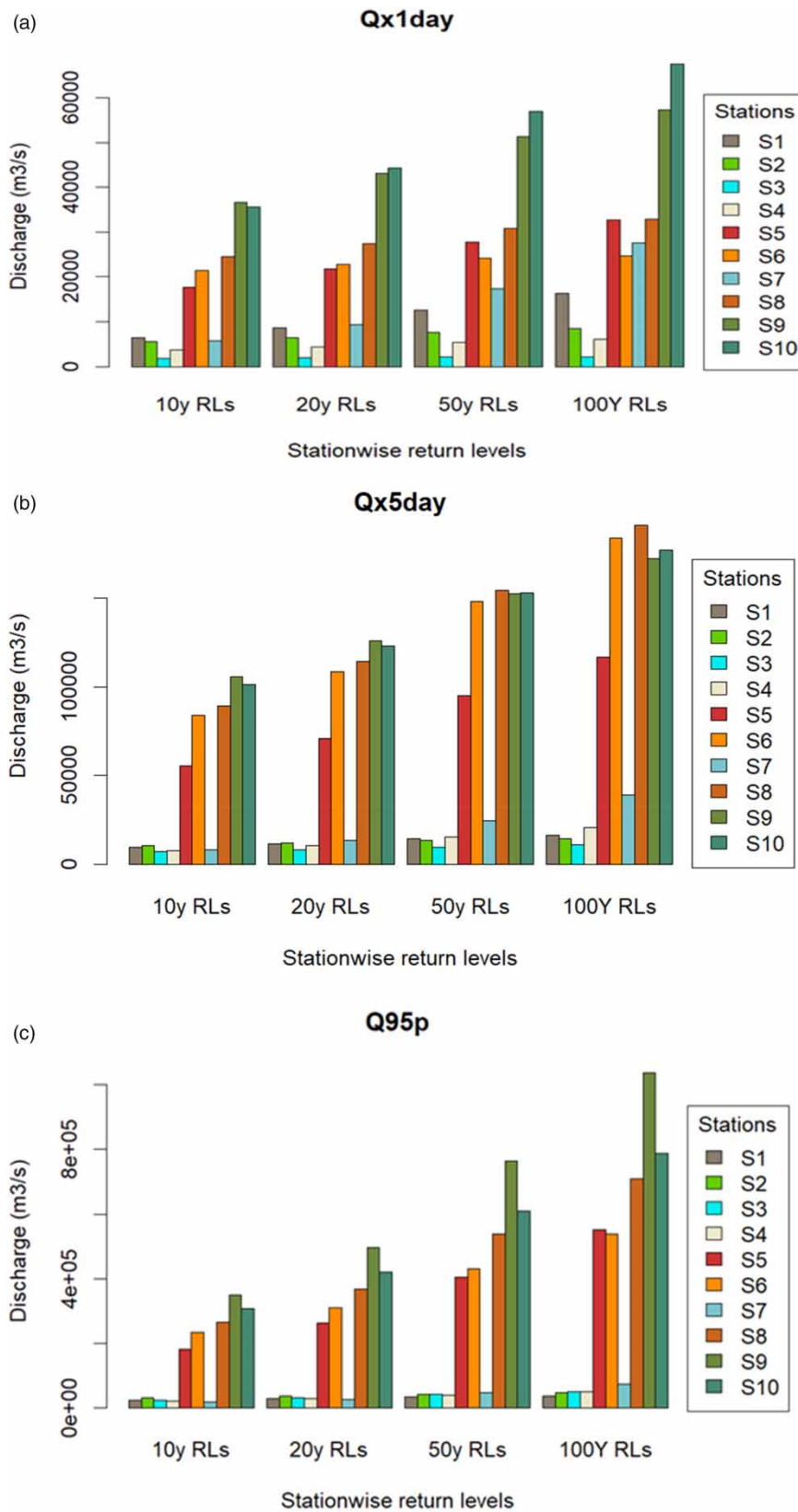
Figure 5 | Continued.
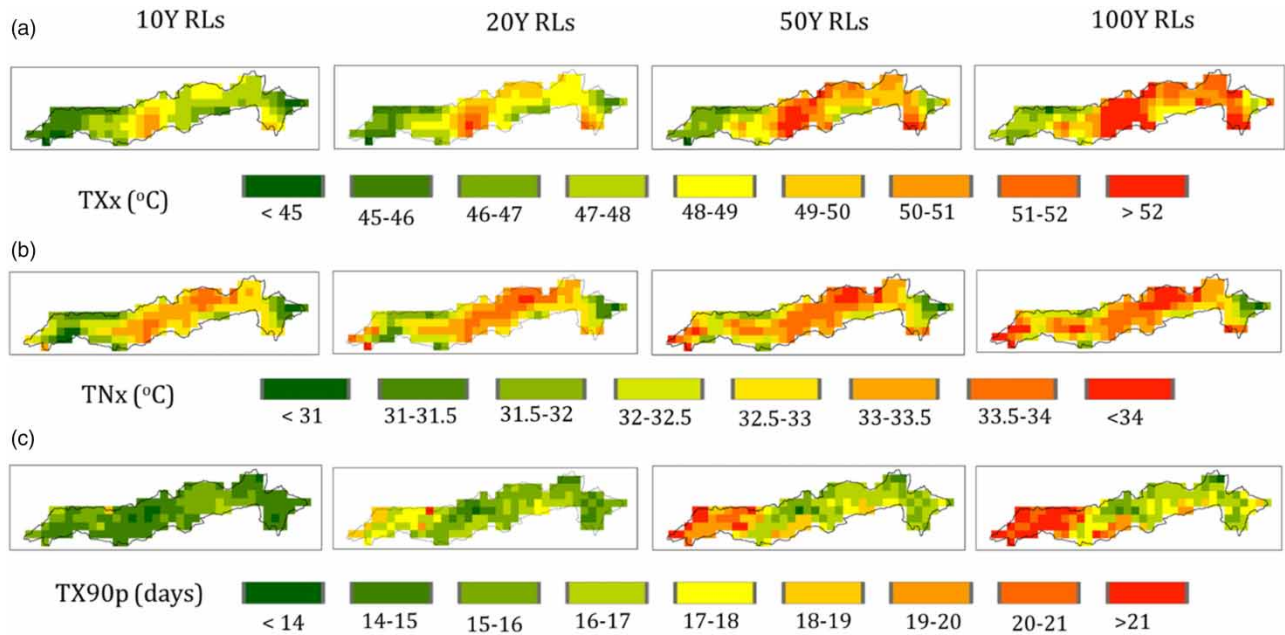
Figure 5 | Continued.

The temperature extremes, TXx, TNx, and TX90p were noticed with significant nonstationary behaviour due to LSCOs throughout the basin (see Supplementary Material, Figure S1). The central upper part of the basin experiences a comparatively higher magnitude of maximum and minimum daily temperature (Figure 5(iii)(a),(b)). The lower part of the basin experiences more number of days with temperatures more than the 90th percentile of daily maximum temperature (T90p) (Figure 5(iii)c).
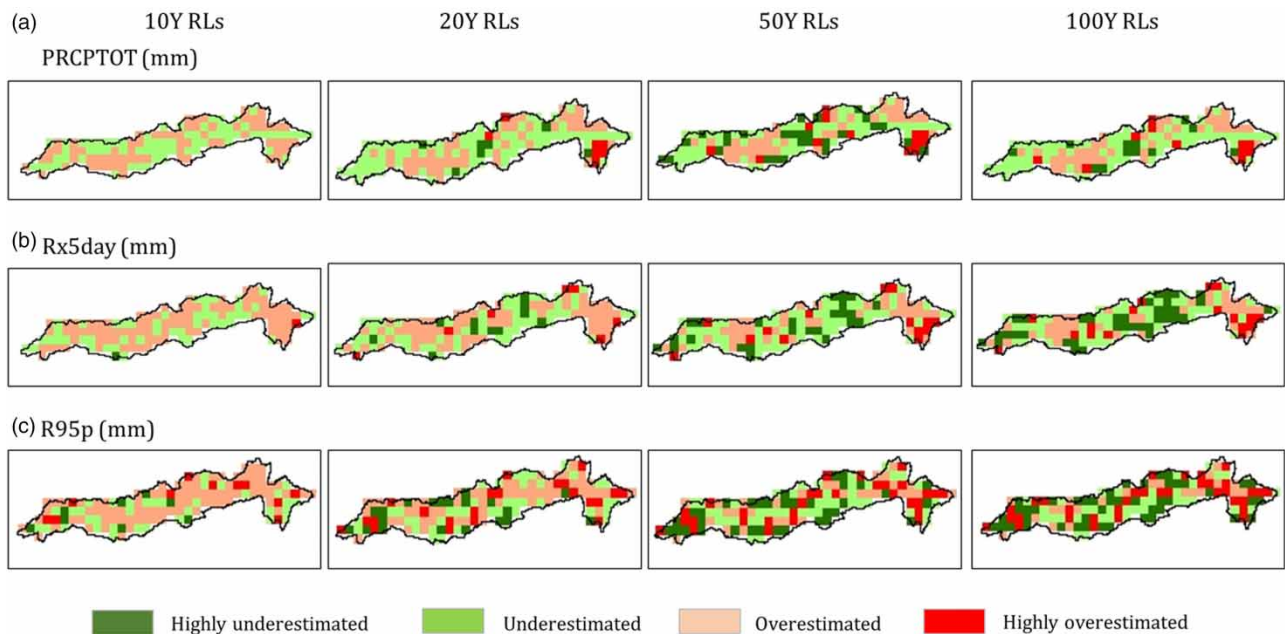
Figure 6 | (i) Difference between return level estimates of stationary (ST) and nonstationary (NS) for precipitation indices: (a) PRCPTOT; (b) Rx5day; and (c) R95p. (ii) Difference between return level estimates of stationary (ST) and nonstationary (NS) for streamflow indices at each station: (a) Q95p; (b) Qx1day; (c) Qx5day. (iii) Difference between return level estimates of stationary (ST) and nonstationary scenario (NS) for temperature indices: (a) TXx; (b) TNx; and (c) TX90p. (continued.).
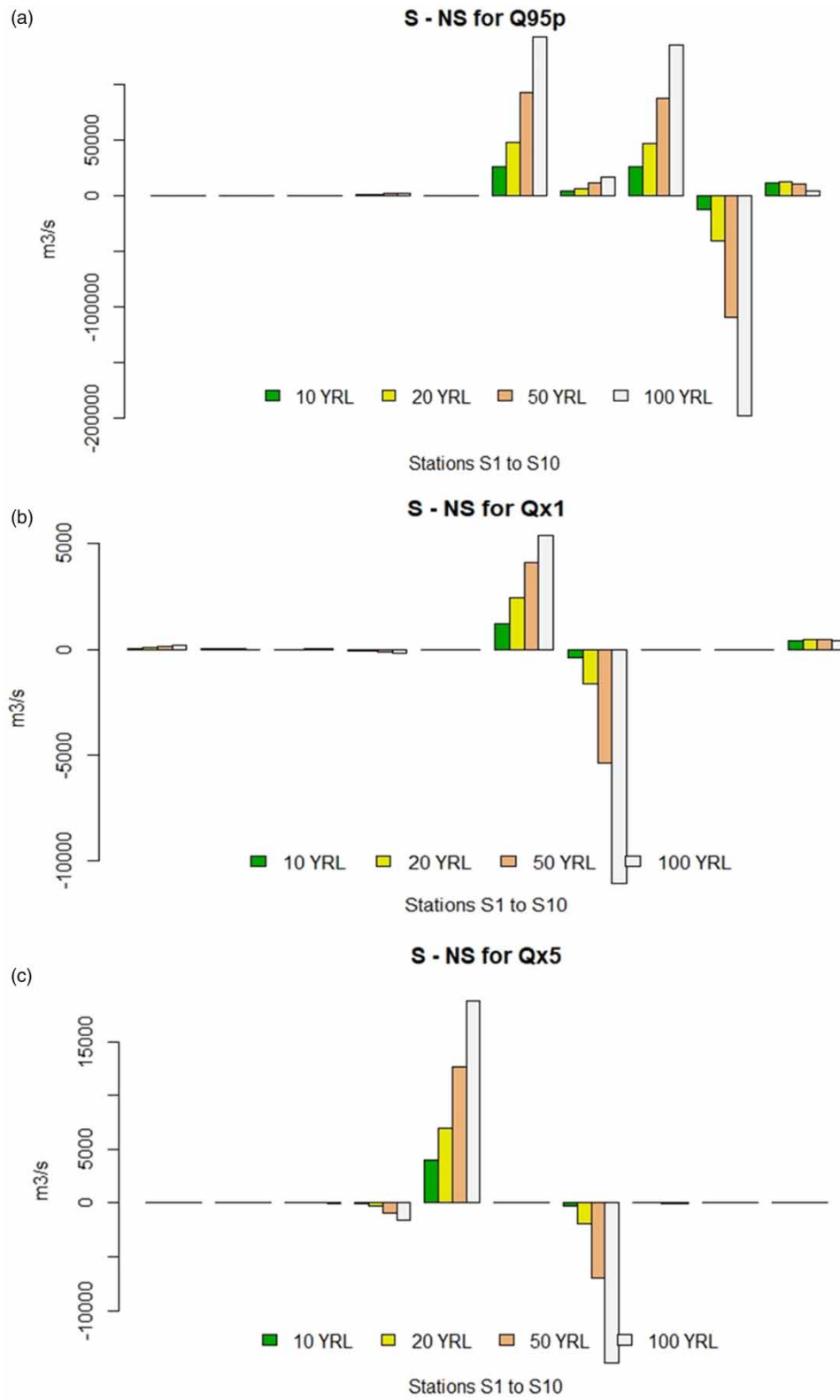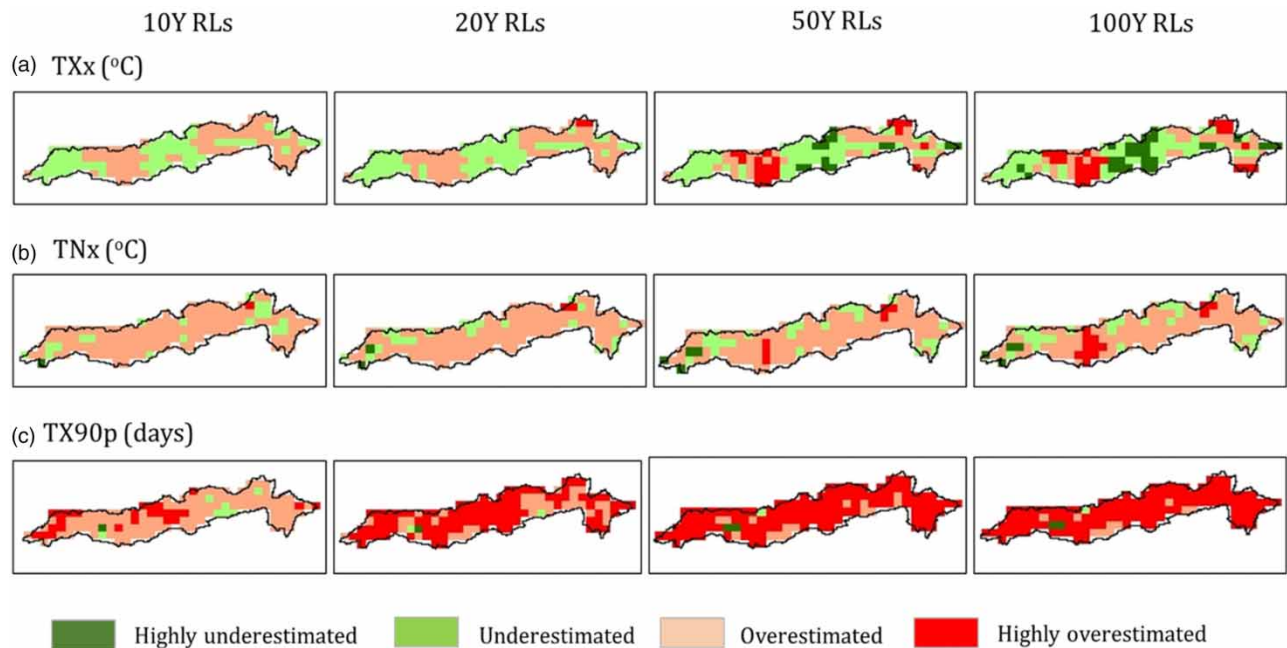
(a)

S - NS for Q95p

(b)

S - NS for Qx1

(c)

S - NS for Qx5

Figure 6 | Continued.

Figure 6 | Continued.

3.2.1. Evaluation of influence of LSCOs

LSCOs either intensify or reduces the magnitude of extremes over various regions of the world. Analysing extremes without considering the effect of LSCOs, either underestimates or overestimates the magnitude of extremes. The possible governing factors in spatiotemporal variability of extremes can be natural variability and anthropogenic forcing (Dai & Bloecker n.d.; Marvel *et al.* 2017). To quantify the degree of influence of LSCOs, we have estimated the differences between extremes in nonstationary scenarios (influenced by the individual or collective response of LSCOs) and stationary scenarios (not getting influenced by LSCOs). The RLs were increasing in magnitude in the case of nonstationary as well stationary analysis with increasing return periods. We observed that at many grids, the returns levels were either overestimated or underestimated with reference to a stationary framework (Figure 6(i)–6(iii)). Conventionally to meet the future requirements of proposed hydraulic structures, the estimation of design capacity is carried out assuming the stationary behaviour of hydroclimatic extremes over a basin. Since the statistical analysis of these extremes as per the available past observations show agreement with significant nonstationary behaviour, the magnitude of these extremes also varies depending on the phases of these LSCOs in many regions. On this ground, the design analysis based on a nonstationary framework makes more realistic sense and hence the projected magnitude of these hydroclimatic extremes in the stationary framework (without getting influenced by LSCOs) gives either underestimated or overestimated value. The underestimation of precipitation and streamflow extremes may lead to under design (capacity) of the hydraulic structure and thus will make it more prone to floods and consequent failure of the structure whereas overestimation of projected magnitude of precipitation and streamflow extremes may lead to overdesign (capacity) of hydraulic structure and this increased projected capacity will increase the cost of the project. Based on the differences in estimates of RLs of both frameworks for all four return periods, the analysis has been carried into four categories: (a) highly underestimated, (b) underestimated, (c) overestimated, and (d) highly overestimated. This classification is based on the concept that if the RLs in the stationary framework give a lesser (higher) value than nonstationary, it means the RLs have been underestimated (overestimated).

Observing the spatiotemporal variation in PRCPTOT, if RLs in the stationary scenario were 100 mm or more amount of deficit in precipitation amount, we have considered as highly underestimated whereas a surplus of 100 or more would be highly overestimated. In case the surplus or deficit of PRCPTOT was lesser than 100 mm, as overestimated and underestimated. From plots (Figure 6(i)(a)), we found that the spatial trend of overestimated or underestimated magnitude of PRCPTOT is similar but increasing with the return period. In the case of Rx5day and R95p, the limit of overestimation and underestimation is taken as 50 and 25 mm, respectively. For all the three precipitation indices, the central part of the

basin experiences underestimated the magnitude of RLs whereas the upper and lower part of the basin experience overestimated RLs.

The difference in RLs of the stationary and nonstationary was plotted for all 10 discharge gauging stations at 10, 20, 50, and 100 return periods (Figure 6(ii)). Qx1day and Qx5day are comparatively instantaneous responses of a river basin whereas Q95p is the comparatively long-term behaviour of a river basin. Therefore, the limits for underestimation/overestimation, in this case, are 1,000, 5,000, and 10,000 m^3/s for Qx1day, Qx5day, and Q95p, respectively. In case of Q95p, for discharge gauging stations, S6 and S10, we got overestimated discharge values, whereas for S6 and S8 RLs were highly overestimated, and at S9, streamflow was highly underestimated. For station S7, Qx1day and Qx5day were highly underestimated for higher return periods whereas, for station S6 and station S5, Qx1day and Qx5day were highly overestimated, respectively, in the stationary framework.

TXx was considered underestimated/overestimated with a decrease/increase by 1 °C/0.5 °C whereas in case of TNx and TX90p a decrease/increase by 0.5 °C/0.5 °C and by 0.5 °C/1 °C, respectively. In case of TXx, RLs were consistently underestimated for some regions and overestimated for others at different return periods. The TNx and TX90p have been found overestimated and highly overestimated in the stationary framework (Figure 6(iii)(b),(c)). This magnitude of overestimated RLs has been found to increase with the return periods (see Supplementary Material, Figure S3).

4. CONCLUSIONS

Hydroclimatic extremes have a significant impact on the hydrological cycle of the basin, such as floods, droughts, or intense precipitation. These events are often caused by complex interactions between atmospheric and hydrological processes and can have severe consequences for water resources and human activities in the affected area. For a major part of the basin, extreme precipitation indices (PRCPTOT, Rx5day, and R95p) were observed to increase but not with any significant trend in the past. The mean values of these precipitation extremes were of higher magnitude at the upper part of the basin whereas the lower part of the basin was showing an increasing trend. In the case of temperature extremes also, the daily maximum temperature was decreasing whereas the daily minimum temperature at annual scale was increasing at the uppermost and lowermost parts of the basin. The temperature extreme, TNx was increasing through the basin whereas in the regions where the daily minimum temperature in a day was increasing, TX90p has been found significantly increasing trend in the past. For streamflow extreme indices (Qx1, Qx5, and Q95p), Z-statistics and Sen's slope from the MK test have been found to decrease for all the 10 discharge gauging stations.

It becomes essential in changing climate to assess the role of local and global factors associated with spatiotemporal variability of hydroclimatic extremes. In this study, we have included major climate oscillations (ENSO, IOD, AMO) in reference to Indian climatology to understand their association with the hydroclimatic extremes at the Narmada basin. The results have been interpreted in two ways: (i) Stationary framework (no influence of LSCOs) and (ii) nonstationary framework (significant influence of LSCOs). The results from the GEV distribution of hydroclimatic extreme indices based on the likelihood ratio test show a significant amount of nonstationarity caused by LSCOs. The precipitation extremes, PRCPTOT and R95p were observed significantly influenced by ENSO, IOD, and AMO individually whereas extreme Rx5day was relatively more influenced by ENSO, and AMO individually and collectively. In terms of temperature extremes, it was shown that TXx in the majority of the Narmada basin (26.47% of the region) was significantly more influenced by ENSO alone, while TNx was observed to be substantially more influenced by ENSO and AMO. Combined with IOD and AMO, ENSO had a considerably greater influence on the temperature extreme TX90p, a potential indicator of heatwaves in a region, and has been noticed with an increasing trend. This linkage may give rise to more frequent and intense heatwaves in the regions which consequently may affect production adversely. By ignoring spatiotemporal variability of extremes caused by ENSO, IOD, and AMO may lead to underestimating and overestimating the magnitude of hydroclimatic extremes of the Narmada basin. The overestimation of RLs will increase the cost of hydraulic projects whereas underestimation may lead to disaster (failure of hydraulic structure) in long term. Some other global and regional factors can also be included in a linear and nonlinear combination of covariates of GEV distribution to better understand the spatiotemporal variability of hydroclimatic extremes. The upper Narmada basin was experiencing a high magnitude of precipitation extremes, hence could be vulnerable to flooding and whereas the basin was projected to experience more frequent and intense heatwave-associated disasters at high return periods. Appropriate adaption and mitigation measures can also be taken to reduce the climate risk in the vulnerable region of the basin.

DATA AVAILABILITY STATEMENT

All relevant data are available from an online repository or repositories.

CONFLICT OF INTEREST

The authors declare there is no conflict.

REFERENCES

Agilan, V. & Umamahesh, N. V. 2018 El Niño southern oscillation cycle indicator for modeling extreme rainfall intensity over India. *Ecological Indicators* **84**, 450–458. https://doi.org/10.1016/j.ecolind.2017.09.012.

AjayaMohan, R. S. & Rao, S. A. 2008 Indian ocean dipole modulates the number of extreme rainfall events over India in a warming environment. *Journal of the Meteorological Society of Japan. Ser. II* **86** (1), 245–252. doi:10.2151/jmsj.86.245.

Alfieri, L., Bisselink, B., Dottori, F., Naumann, G., de Roo, A., Salamon, P., Wyser, K. & Feyen, L. 2017 Global projections of river flood risk in a warmer world. *Earths Future* **5** (2), 171–182. Wiley Online Library.

Ashok, K., Guan, Z. & Yamagata, T. 2001 Impact of the Indian Ocean dipole on the relationship between the Indian monsoon rainfall and ENSO. *Geophysical Research Letters* **28** (23), 4499–4502. John Wiley & Sons, Ltd. https://doi.org/10.1029/2001GL013294.

Beniston, M. 2015 Ratios of record high to record low temperatures in Europe exhibit sharp increases since 2000 despite a slowdown in the rise of mean temperatures. *Climate Change* **129**, 225–237.

Bracken, C., Holman, K. D., Rajagopalan, B. & Moradkhani, H. 2018 A Bayesian hierarchical approach to multivariate nonstationary hydrologic frequency analysis. *Water Resources Research* **54** (1), 243–255. John Wiley & Sons, Ltd. https://doi.org/10.1002/2017WR020403.

Canadell, J. G., Monteiro, P. M. S., Costa, M. H., Cotrim da Cunha, L., Cox, P. M., Eliseev, A. V., Henson, S., Ishii, M., Jaccard, S., Koven, C., Lohila, A., Patra, P. K., Piao, S., Rogelj, J., Syampungani, S., Zaehle, S. & Zickfeld, K. 2021 Global carbon and other biogeochemical cycles and feedbacks. In: *Climate Change 2021: The Physical Science Basis* (V. Masson-Delmotte, P. Zhai, A. Pirani, S. L. Connors, C. Péan, S. Berger, N. Caud, Y. Chen, L. Goldfarb, M. I. Gomis, M. Huang, K. Leitzell, E. Lonnoy, J. B. R. Matthews, T. K. Maycock, T. Waterfield, O. Yelekçi, R. Yu & B. Zhou, eds). Contribution of Working Group I to the Sixth Assessment Report of the Intergovernmental Panel on Climate Change. Cambridge University Press, Cambridge, UK and New York, NY, USA, pp. 673–816. doi:10.1017/9781009157896.007.

Coles, S. 2001 *An Introduction to Statistical Modeling of Extreme Values*. Springer. Available from: https://link.springer.com/book/10.1007%2F978-1-4471-3675-0.

Coumou, D., Robinson, A. & Rahmstorf, S. 2013 Global increase in record-breaking monthly-mean temperatures. *Climate Change* **118**, 771–782.

Dai, A. 2011 Drought under global warming: a review. *Wiley Interdisciplinary Reviews: Climate Change* **2** (1), 45–65. Wiley Online Library.

Dai, A. & Bloecker, C. E. n.d. Impacts of internal variability on temperature and precipitation trends in large ensemble simulations by two climate models. *Climate Dynamics* **52** (1–2), 289–306. Germany. doi:101007/s00382-018-4132-4.

Das, J., Jha, S. & Goyal, M. K. 2020 Non-stationary and copula-based approach to assess the drought characteristics encompassing climate indices over the Himalayan states in India. *Journal of Hydrology (Amsterdam)* **580**, 124356. https://doi.org/10.1016/j.jhydrol.2019.124356.

Dosio, A., Mentaschi, L., Fischer, E. M. & Wyser, K. 2018 Extreme heat waves under 1.5 C and 2 C global warming. *Environmental Research Letters* **13** (5), 54006. IOP Publishing.

Field, C. B., Barros, V., Stocker, T. F. & Dahe, Q. 2012 Managing the risks of extreme events and disasters to advance climate change adaptation. *Special Report of the Intergovernmental Panel on Climate Change*. Cambridge University Press, Cambridge, UK, and New York, NY, USA, 582 pp.

Gao, T., Wang, H. J. & Zhou, T. 2017 Changes of extreme precipitation and nonlinear influence of climate variables over monsoon region in China. *Atmospheric Research* **197**, 379–389. https://doi.org/10.1016/j.atmosres.2017.07.017.

Garner, G., Van Loon, A. F., Prudhomme, C. & Hannah, D. M. 2015 Hydroclimatology of extreme river flows. *Freshwater Biology* **60** (12), 2461–2476. John Wiley & Sons, Ltd. https://doi.org/10.1111/fwb.12667.

Goswami, U. P., Hazra, B. & Goyal, M. K. 2018 Copula-based probabilistic characterization of precipitation extremes over North Sikkim Himalaya. *Atmospheric Research* **212**, 273–284. doi:10.1016/j.atmosres.2018.05.019.

Hirabayashi, Y., Kanae, S., Emori, S., Oki, T. & Kimoto, M. 2008 Global projections of changing risks of floods and droughts in a changing climate. *Hydrological Sciences Journal* **53** (4), 754–772. Taylor & Francis. doi:10.1623/hysj.53.4.754.

India-WRIS 2012 *River Basin Atlas of India*. RRSC-West, NRSC, ISRO, Jodhpur, India.

Jha, S., Das, J. & Goyal, M. K. 2021 Low frequency global-scale modes and its influence on rainfall extremes over India: nonstationary and uncertainty analysis. *International Journal of Climatology* **41** (3), 1873–1888. John Wiley & Sons, Ltd. https://doi.org/10.1002/joc.6935.

Katz, R. W. 2013 Statistical methods for nonstationary extremes. In: *Extremes in a Changing Climate*. Springer, Dordrecht, pp. 15–37. https://doi.org/10.1007/978-94-007-4479-0_2.

Khaki, M., Awange, J., Forootan, E. & Kuhn, M. 2018 Understanding the association between climate variability and the Nile's water level fluctuations and water storage changes during 1992–2016. *Science of The Total Environment* **645**, 1509–1521. https://doi.org/10.1016/j.scitotenv.2018.07.212.

Krishna, K. K., Balaji, R. & Cane, M. A. 1999 On the weakening relationship between the Indian monsoon and ENSO. *Science (1979)* **284** (5423), 2156–2159. American Association for the Advancement of Science. doi:10.1126/science.284.5423.2156.

Maity, R., Kumar, D. N. & Nanjundiah, R. S. 2007 Review of hydroclimatic teleconnection between hydrologic variables and large-scale atmospheric circulation patterns with Indian perspective. *ISH Journal of Hydraulic Engineering* **13** (1), 77–92. Taylor & Francis. doi:10.1080/09715010.2007.10514859.

Marvel, K., Biasutti, M., Bonfils, C., Taylor, K., Kushnir, Y. & Cook, B. 2017 Observed and projected changes to the precipitation annual cycle. *Journal of Climate* **30**. doi:10.1175/JCLI-D-16-0572.1.

Naumann, G., Alfieri, L., Wyser, K., Mentaschi, L., Betts, R. A., Carrao, H., Spinoni, J., Vogt, J. & Feyen, L. 2018 Global changes in drought conditions under different levels of warming. *Geophysical Research Letters* **45** (7), 3285–3296. Wiley Online Library.

Naveendrakumar, G., Vithanage, M., Kwon, H.-H., Chandrasekara, S. S. K., Iqbal, M. C. M., Pathmarajah, S., Fernando, W. C. D. K. & Obeysekera, J. 2019 South Asian perspective on temperature and rainfall extremes: A review. *Atmospheric Research* **225**, 110–120.

Ouarda, T. B. M. J. & Charron, C. 2019 Changes in the distribution of hydro-climatic extremes in a non-stationary framework. *Scientific Reports* **9** (1), 8104. doi:10.1038/s41598-019-44603-7.

Panda, D. K., Kumar, A., Ghosh, S. & Mohanty, R. K. 2013 Streamflow trends in the Mahanadi River basin (India): linkages to tropical climate variability. *Journal of Hydrology (Amsterdam)* **495**, 135–149. https://doi.org/10.1016/j.jhydrol.2013.04.054.

Parey, S., Hoang, T. T. H. & Dacunha-Castelle, D. 2010 Different ways to compute temperature return levels in the climate change context. *Environmetrics* **21** (7–8), 698–718. John Wiley & Sons, Ltd. https://doi.org/10.1002/env.1060.

Pechlivanidis, I. G., Arheimer, B., Donnelly, C., Hundecha, Y., Huang, S., Aich, V., Samaniego, L., Eisner, S. & Shi, P. 2017 Analysis of hydrological extremes at different hydro-climatic regimes under present and future conditions. *Climate Change* **141** (3), 467–481. Climatic Change. doi:10.1007/s10584-016-1723-0.

Ratna, S. B., Cherchi, A., Osborn, T. J., Joshi, M. & Uppara, U. 2021 The extreme positive Indian ocean dipole of 2019 and associated Indian summer monsoon rainfall response. *Geophysical Research Letters* **48** (2), e2020GL091497. John Wiley & Sons, Ltd. https://doi.org/10.1029/2020GL091497.

Rose, L. S. & LaRow, T. 2016 The relationship between climate oscillations and regional extremes. In *AGU Fall Meeting Abstracts*. Vol. 2016, A23H-0320.

Rummukainen, M. 2012 Changes in climate and weather extremes in the 21st century. *Wiley Interdisciplinary Reviews: Climate Change* **3** (2), 115–129. Wiley Online Library.

Russo, S., Sillmann, J. & Fischer, E. M. 2015 Top ten European heatwaves since 1950 and their occurrence in the coming decades. *Environmental Research Letters* **10** (12), 124003. IOP Publishing. doi:10.1088/1748-9326/10/12/124003.

Sahu, N., Behera, S. K., Yamashiki, Y., Takara, K. & Yamagata, T. 2012 IOD and ENSO impacts on the extreme stream-flows of citarum river in Indonesia. *Climate Dynamics* **39** (7), 1673–1680. doi:10.1007/s00382-011-1158-2.

Saji, N. H., Goswami, B. N., Vinayachandran, P. N. & Yamagata, T. 1999 A dipole mode in the tropical Indian Ocean. *Nature* **401** (6751), 360–363. doi:10.1038/43854.

Salas, J. & Obeysekera, J. 2014 Revisiting the concepts of return period and risk for nonstationary hydrologic extreme events. *Journal of Hydrologic Engineering* **19**, 554–568.

Schär, C., Ban, N., Fischer, E., Rajczak, J., Schmidli, J., Frei, C., Giorgi, F., Karl, T. R., Kendon, E., Tank, A., O'Gorman, P., Sillmann, J., Zhang, X. & Zwiers, F. 2016 Percentile indices for assessing changes in heavy precipitation events. *Climate Change* **137**. doi:10.1007/s10584-016-1669-2.

Seo, S. B., Kim, Y.-O., Kim, Y. & Eum, H.-I. 2019 Selecting climate change scenarios for regional hydrologic impact studies based on climate extremes indices. *Climate Dynamics* **52** (3–4), 1595–1611. Germany. doi:101007/s00382-018-4210-7.

Sharma, S. & Mujumdar, P. 2017 Increasing frequency and spatial extent of concurrent meteorological droughts and heatwaves in India. *Scientific Reports* **7** (1), 15582. doi:10.1038/s41598-017-15896-3.

Singh, S., Prasad, B. & Tiwari, H. L. 2021 Sedimentation analysis for a reservoir using remote sensing and GIS techniques. *ISH Journal of Hydraulic Engineering*, 1–9. Taylor & Francis. doi:10.1080/09715010.2021.1975318.

Singh, S., Goyal, M. K. & Jha, S. 2023 Role of large-scale climate oscillations in precipitation extremes associated with atmospheric rivers: nonstationary framework. *Hydrological Sciences Journal*. Taylor & Francis. doi:10.1080/02626667.2022.2159412.

Song, X., Zhang, J., Zou, X., Zhang, C., AghaKouchak, A. & Kong, F. 2019 Changes in precipitation extremes in the Beijing metropolitan area during 1960–2012. *Atmospheric Research* **222**, 134–153. https://doi.org/10.1016/j.atmosres.2019.02.006.

Thomas, T., Gunthe, S. S., Sudheer, K. P. & Ghosh, N. C. 2015 Analysis of monsoon rainfall variability over Narmada basin in central India: implication of climate change. *Journal of Water and Climate Change* **6** (3), 615–627. doi:10.2166/wcc.2014.041.

Trenberth, K. E. & Fasullo, J. T. 2012 Climate extremes and climate change: the Russian heat wave and other climate extremes of 2010. *Journal of Geophysical Research: Atmospheres* **117** (D17). John Wiley & Sons, Ltd. https://doi.org/10.1029/2012JD018020.

Trenberth, K. E. & Guillemot, C. J. 1996 Physical processes involved in the 1988 drought and 1993 floods in North America. *Journal of Climate* **9**, 1288–1298. doi:10.1175/1520-0442(1996)009 < 1288:PPIITD > 2.0.CO;2.

Vinayachandran, P. N., Iizuka, S. & Yamagata, T. 2002 Indian ocean dipole mode events in an ocean general circulation model. *Deep-sea Research Part Ii-Topical Studies in Oceanography* **49**, 1573–1596.

Vittal, H., Villarini, G. & Zhang, W. 2020 Early prediction of the Indian summer monsoon rainfall by the Atlantic Meridional Mode. *Climate Dynamics* **54**, 2337–2346.

Ward, P. J., Eisner, S., Flörke, M., Dettinger, M. D. & Kummu, M. 2014 Annual flood sensitivities to El Niño–Southern oscillation at the global scale. *Hydrology and Earth System Sciences* **18** (1), 47–66. doi:10.5194/hess-18-47-2014.

Yilmaz, A. G. & Perera, B. J. C. 2014 Extreme rainfall nonstationarity investigation and Intensity–Frequency–Duration relationship. *Journal of Hydrologic Engineering* **19** (6), 1160–1172. American Society of Civil Engineers. doi:10.1061/(ASCE)HE.1943-5584.0000878.